

## The Effects of Substrate Phonon Mode Scattering on Transport in Carbon Nanotubes

Vasili Perebeinos<sup>1</sup>, Slava Rotkin<sup>2</sup>, Alexey G. Petrov<sup>3</sup>, and Phaedon Avouris<sup>1</sup><sup>1</sup>IBM Research Division, T. J. Watson Research Center,  
Yorktown Heights, New York 10598<sup>2</sup>Physics Department, Lehigh University, 16 Memorial Dr. E., Bethlehem, PA 18015Center for Advanced Materials and Nanotechnology,  
Lehigh University, 5 E. Packer Ave., Bethlehem, PA 18015<sup>3</sup>Tole Institute, 26 Polytekhnicheskaya, St. Petersburg, 194021, Russia

(Dated: February 21, 2024)

Carbon nanotubes (CNTs) have large intrinsic carrier mobility due to weak acoustic phonon scattering. However, unlike two-dimensional metal-oxide-semiconductor field effect transistors (MOS-FETs), substrate surface polar phonon (SPP) scattering has a dramatic effect on the CNT FET mobility, due to the reduced vertical dimensions of the latter. We find that for the Van der Waals distance between CNT and an  $\text{SiO}_2$  substrate, the low-field mobility at room temperature is reduced by almost an order of magnitude depending on the tube diameter. We predict additional experimental signatures of the SPP mechanism in dependence of the mobility on density, temperature, tube diameter, and CNT-substrate separation.

Semiconducting carbon nanotubes (CNTs) show promise for technological applications in electronics and optoelectronics primarily due to weak acoustic phonon carrier scattering and a direct bandgap [1]. The low-field mobilities in CNTs have been measured by several groups [2, 3, 4]. At low biases only acoustic phonons contribute to the scattering in CNTs and the scattering is weak [5, 6, 7]. The CNT diameter  $d$  scaling of the low-field mobility was predicted [7] to be  $\propto d^2$  and confirmed experimentally [3]. However, the magnitude of the experimental mobility was found to be an order of magnitude smaller than the theoretical prediction. Recently it was shown that surface polar phonon (SPP) scattering can be strong in CNTs lying on polar substrates such as  $\text{SiO}_2$  [8]. While the SPP scattering is of lesser importance in the conventional two-dimensional MOSFETs [9], as we show below it is much more prominent in CNTs due to the much smaller vertical dimension of the devices given by the CNT diameter.

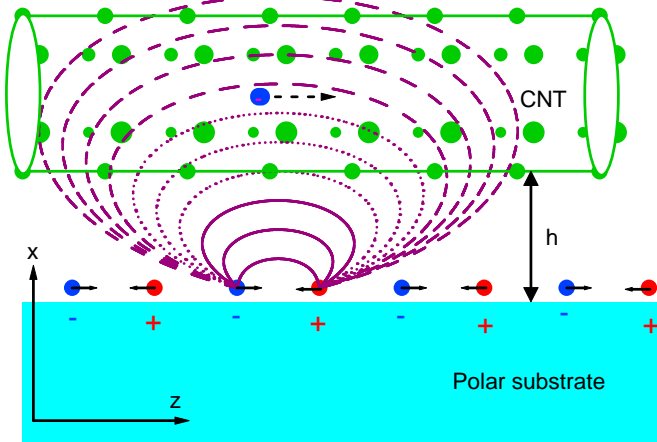


FIG. 1: Schematics of the SPP scattering in CNTs.

In this Letter we evaluate the transport properties of CNTs due to the extrinsic scattering mechanism by surface phonons in the insulating polar substrates as schematically shown in Fig. 1. The surface phonons on polar substrates produce a surface electric field coupled to the electrons on the nearby CNTs. We find that SPP scattering lowers dramatically the low-field mobility, even at room temperature. What is more surprising, the SPP scattering can increase the drift velocity under high bias conditions, especially at high doping levels and elevated CNT phonon temperatures.

The interaction potential is given by [10]:

$$V_{\text{int}} = e \frac{\tilde{R}}{\tilde{r}} \frac{\tilde{r}}{3} \tilde{P}(\tilde{R}) \quad (1)$$

where  $\tilde{R}$  and  $\tilde{r}$  are substrate phonon and CNT electron coordinates, respectively. The strength of the SPP scattering is given by the polarization field  $\tilde{P}(\tilde{R})$  at the surface associated with a particular excited phonon mode:

$$\tilde{P}(\tilde{R}) = \sum_{\mathbf{q}} F \frac{\tilde{r}}{A} \frac{\tilde{r}}{A} e^{i(\mathbf{q} \cdot \tilde{\mathbf{r}} + i\mathbf{q} \cdot \tilde{\mathbf{R}})} (\hat{\mathbf{q}} \cdot i\hat{\mathbf{x}}) a_{\mathbf{q}}^y + \text{h.c.} \quad (2)$$

where  $a_{\mathbf{q}}^y$  is a creation operator of a surface phonon mode with two-dimensional wavevector  $\mathbf{q}$ . The vector normal to the solid (at  $x < 0$ ) is  $\hat{\mathbf{x}}$  and the unit vector along  $\mathbf{q}$  is  $\hat{\mathbf{q}}$ . The normalization surface area  $A$  drops out from the final result. The magnitude of the polarization field is controlled by the Frohlich coupling  $F$ :

$$F^2 = \frac{\epsilon_{\text{so}}}{2} \frac{1}{\epsilon_1 + 1} \frac{1}{\epsilon_0 + 1}; \quad (3)$$

where  $\epsilon_{\text{so}}$  is a surface phonon energy and  $\epsilon_0$  and  $\epsilon_1$  are the low- and high-frequency dielectric constants of the

polar substrate [11]. In the following we evaluate scattering in CNTs on  $\text{SiO}_2$  surfaces, which have five phonon modes  $\sim \omega_{\text{SPP}} = 50; 62; 100; 149; 149$  meV, with Frohlich couplings  $F_{1\ldots 5}^2 = 0.042; 0.38; 0.069; 1.08; 1.08$  meV respectively [12].

The CNT electron-polar surface phonon matrix element has been derived in the envelope wavefunction approximation in [8]:

$$M_{kq}^2 = \frac{\hbar^2}{L} \frac{4e^2 F^2}{I_m^2} \frac{q_z d}{2} K_{2m}((d+2h)q_z) \quad (4)$$

where  $\psi_k$  and  $\psi_{k+q}$  are electron wavefunctions in CNT with momentum  $k$  and  $k+q$  characterized by the quantized angular momentum  $m$  and a continuous  $z$  component along the tube axis,  $d$  is a tube diameter, and  $h$  is the height from the CNT surface to the insulating substrate, see Fig. 1. The length of the tube  $L$  determines the  $k$ -point sampling along the tube axis  $q_z = 2\pi/L$ . The functions  $I$  and  $K$  are the Bessel functions of the first and second order, respectively. It was shown that SPP scattering is strongest when the azimuthal angular momentum is conserved,  $m = 0$  [8]. Therefore, to analyze the results of the calculations it is instructive to consider the asymptotic form of the scattering potential for  $m = 0$  and large  $q_z$ :

$$M_{kq}^2 \approx \frac{4e^2 F^2}{L} \frac{e^{2hq_z}}{q_z d^2 (d+2h)} \quad (5)$$

This form of the SPP coupling also works well for the intermediate values of  $q_z$ .

The electron-CNT phonon scattering is described using the Su-Schrieffer-Heger model as in ref. [7] with the coupling constant  $g = 5.3$  eV/Å. The electron band structure is described by the  $\pi$ -orbital tight-binding model with  $t_0 = 3$  eV.

We study the effect of the SPP scattering on transport in the diffusive regime. We calculate the mobility by solving the steady-state multiband Boltzmann transport equation (BTE) in the presence of an electric field. The temperature dependent scattering rates  $W_{k;k+q}$  between electronic states  $k$  and  $k+q$  entering in the BTE equation are evaluated according to:

$$W_{k;k+q} = \frac{2}{\hbar} \sum_q M_{kq}^2 n_q [f_k - f_{k+q + \omega_q}] + (1 + n_q) [f_k - f_{k+q - \omega_q}] \quad (6)$$

where the phonon occupation number  $n_q$  is given by the Bose-Einstein distribution. The phonon index runs over all phonon modes involved in scattering, i.e. six CNT phonon modes and five surface phonon modes in  $\text{SiO}_2$ , the latter are treated here as being dispersiveless.

The inverse mobility at low-field and low density is shown in Fig. 2 as a function of temperature. At low

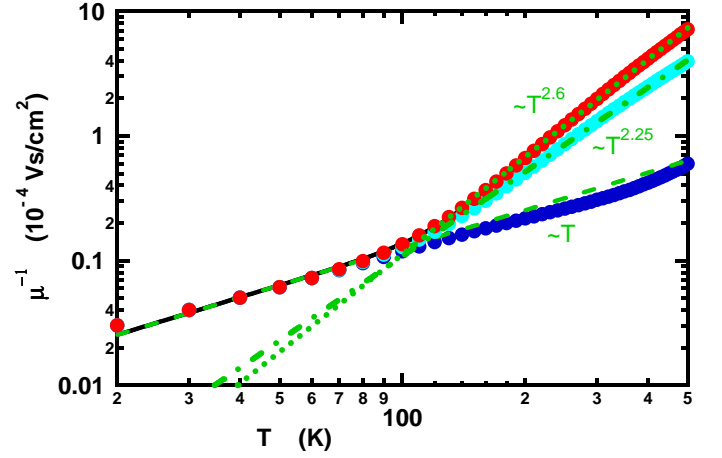


FIG. 2: Temperature dependence of the low-field, low-density inverse mobility in (19,0) tube ( $d = 1.5$  nm) on a log-log scale. The red circles are in the presence of both CNT phonons and the SPP scattering, the cyan circles with CNT phonons and one surface phonon at  $\sim \omega_{12} = 62$  meV, blue circles with the CNT phonon scattering alone. The black solid curve is a fit to Eq. (7) with  $\text{CNT} = 0.0013$  and  $\text{SPP} = 13.4$ . The low temperature mobility is influenced by the CNT acoustic phonon scattering and gives linear temperature dependence shown by the green dashed line. The high temperature inverse mobility can be approximated by the power-laws shown by the green dashed ( $T^{2.6}$ ) and dashed-dotted lines ( $T^{2.25}$ ).

temperatures, the inverse mobility is linear in temperature, because only CNT acoustic phonon scattering dominates transport in that regime. At temperatures above about  $T = 100$  K, SPP scattering is activated and starts to dominate transport. The temperature dependence of the low-field mobility becomes superlinear, due to the activated nature of the SPP scattering and can well be approximated by the following formula:

$$\mu^{-1} = \text{CNT} T + \text{pol}(n_B(\sim \omega_{12}) + n_B(\sim \omega_{4,5})); \quad (7)$$

where  $\text{CNT}$  is a contribution from the acoustic CNT phonons and  $\text{SPP}$  is proportional to the SPP scattering rate,  $n_B$  is the occupation number of SPP with energies  $\sim \omega_{12} = 62$  meV,  $\sim \omega_{4,5} = 149$  meV, and  $\text{pol} = (F_4^2 + F_5^2)/F_2^2 = 5.6$  is the ratio of the electron-polar phonon coupling strengths fixed by the ratio of the Frohlich couplings. Since the occupation number of the highest energy SPP phonon of 149 meV is much smaller than the  $\sim \omega_{12} = 62$  meV mode, in a zeroth order approximation the mobility below room temperature can be calculated through a coupling only to the 62 meV SPP phonon mode. We note however that this approximation is not exact and at least the two lowest energy modes  $\sim \omega_{11}$  and  $\sim \omega_{12}$  have to be included to get an adequate mobility at room temperatures. The single mode  $\sim \omega_{12}$  calculations shown in Fig. 2 (cyan color) overestimate mobility by 50% at room temperature.

Despite the fact that the two low energy SPP phonons

at room temperature have small occupations of  $n_B = 0.15$  and  $0.09$  respectively, they dominate the mobility, because of much stronger coupling than that to CNT acoustic phonons. The mobility at room temperature degrades by an order of magnitude in the presence of the SPP mechanism, depending on the tube diameter and its distance from the substrate surface  $h$ . The latter depends ultimately on the roughness of the surface. The low-field mobility dependence on  $h$  can be rationalized by Matthiessen's rule, with the SPP scattering rate given by Eq. (5) and CNT phonon scattering described by the mobility  $\mu_{CNT}$  in isolated (suspended) CNT:

$$\mu = \frac{\mu_{CNT}}{1 + (\mu_{CNT} = \mu_{SiO_2})^{-1} e^{(2q_z(h-h_0)) \frac{d+2h_0}{d+2h}}}; \quad (8)$$

where  $\mu_{SiO_2}$  is mobility on polar surface substrates with the minimum distance determined by the Van der Waals interaction  $h_0 = 0.35$  nm. The electron momentum transfer along the tube axis is the scattering of a surface phonon is given by  $\sim v_F q_z = \frac{1}{2} (2 + \frac{1}{2})$ , where  $2.09 = d$  eV nm is a bandgap and  $v_F = 10^8$  cm/s is the Fermi velocity. We find that the ratio of the low-field mobilities at room temperature can be as large as a factor of 8.6 in 2.5 nm diameter tubes.

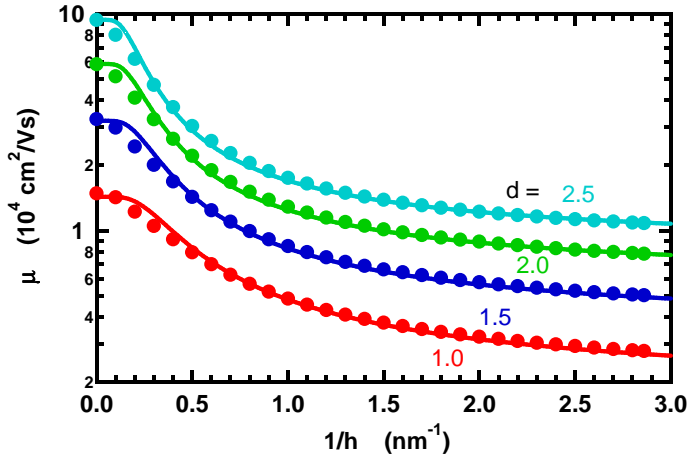


FIG. 3: Dependence of the low-field, low-density mobility on the inverse distance from the polar substrate at room temperature on a logarithmic scale. The mobility is reduced by a factor of  $\mu_{CNT} = \mu_{SiO_2} = 5.3, 6.5, 7.5$ , and  $8.6$  correspondingly in (1.0, 0) -red, (1.5, 0) -blue, (2.0, 0) -green, and (2.5, 0) -cyan tubes. The solid curves are calculations according to Eq. (8) with  $q_z = 0.38, 0.32, 0.28$ , and  $0.25$  nm $^{-1}$ .

The diameter dependence of the low-field, low-density mobility shows a power law behavior:

$$\mu(d) = A d^\alpha; \quad (9)$$

with power  $\alpha$  being temperature dependent as shown in Fig. 4. At low temperatures, only acoustic phonons in the CNT contribute to the scattering and the power is  $\alpha = 2$

as found in ref. [3, 7] and Fig. 3 in Supporting Information. At higher temperatures, SPP scattering contributes to mobility with a weaker diameter dependence than that for CNT phonons. This results in smaller  $\alpha$  in Eq. (9) at elevated temperatures. Therefore, the relative contribution to the total mobility of the SPP phonons in Fig. 3 is larger in larger diameter tubes, i.e.  $\mu_{CNT} = \mu_{SiO_2} / d^{0.5}$  at  $T = 300$  K and  $\mu_{CNT} = \mu_{SiO_2} / d^{0.7}$  at  $T = 500$  K.

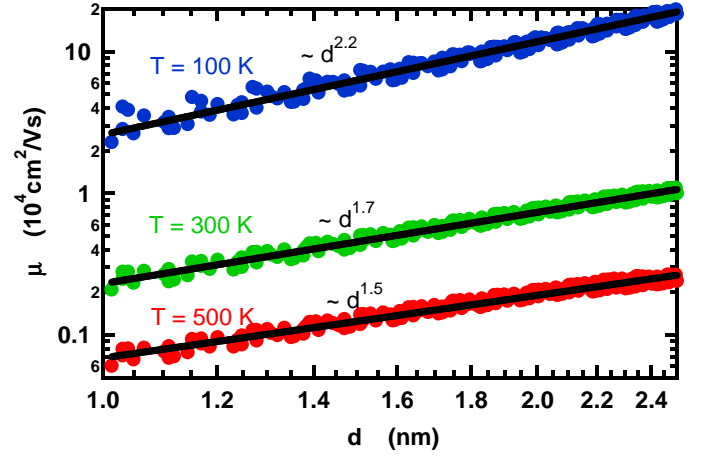


FIG. 4: Low-field, low-density mobility as a function of tube diameter at three temperatures on a log-log plot for all chirality tubes. The black solid lines are best fits to Eq. (9) with  $(A; \alpha) = (2.6, 2.18)$ ,  $(0.23, 1.67)$ , and  $(0.069, 1.47)$  for  $T = 100$  K -blue,  $T = 300$  -green, and  $T = 500$  -red respectively.

Although it is natural to analyze low-density mobility theoretically, it is difficult to measure it experimentally because the device is close to the  $\phi$ -state with a high resistance. In the case of only CNT phonon scattering, as the device is electrostatically or chemically doped with carriers, the mobility was shown to increase due to the smaller density of states available for scattering as the Fermi level moves away from the bottom of the conduction or valence bands [13]. As the Fermi level approaches the second band, a new channel for scattering opens up and the mobility drops showing a non-monotonic behavior. In the presence of the SPP scattering, the density dependence of the mobility shows an additional minimum, when the Fermi level approaches the lowest energy SPP phonon energy  $\sim \frac{1}{2}$  with the strongest coupling, as shown in Fig. 5a. The size of the mobility modulation depends on the temperature  $T$ , which determines the Pauli blocking factors  $(1 - g_k) = e^{E_{Fermi} - E_k / k_B T}$ , where  $g_k$  is the distribution function from the BTE solution and  $E_{Fermi}$  is the quasi-Fermi level. At low temperatures  $T = 100$  K, the Pauli blocking principle does not allow any SPP scattering even if the energy conservation law can be satisfied  $E_{Fermi} \sim \frac{1}{2}$ . At higher temperatures the mobility minimum broadens out with increasing temperature. As the density further increases, the mobility increases until it reaches the bottom of the second band, showing a second

minimum associated with the higher subband scattering [13].

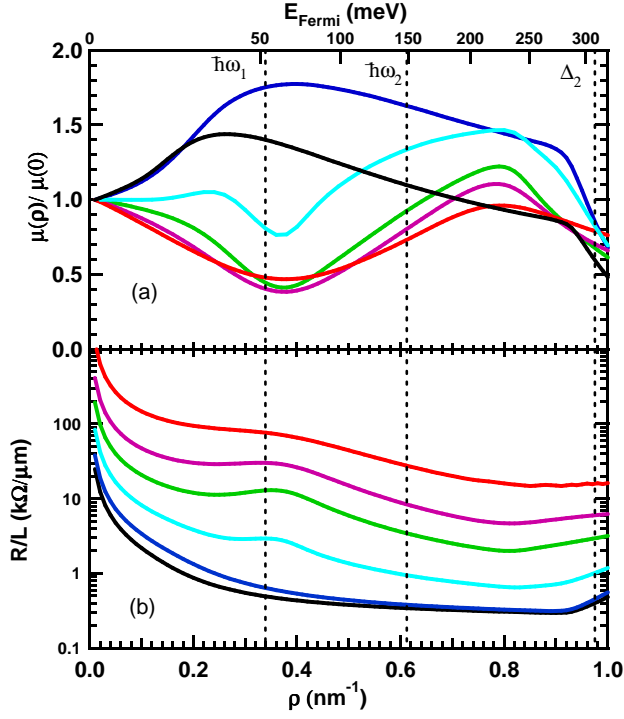


FIG. 5: (a) Carrier density dependence of the low-field mobility in the same tube normalized to its value at zero density. The vertical lines show energies of the two polar optical phonons and the second subband, at which scattering time is being reduced. The upper axis shows the energy of the Fermi levels for a given density at zero temperature. (b) Resistance per unit length in (19,0) tube ( $d = 1.5$  nm) at different temperatures 30 K (black), 50 K (blue), 100 K (cyan), 150 K (green), 200 K (magenta), 300 K (red) on a log scale.

We have calculated the dependence of the resistivity on carrier density for the same tube and the results are shown in Fig. 5b. The resistivity (resistance per CNT tube length) is non-monotonic with a minimum corresponding to occupation of the second subband at low temperatures and a second minimum emerging at intermediate temperatures  $T \sim 100$  K due to the SPP scattering. The prediction of the appearance of a second minimum in the resistivity at higher temperatures could provide an experimental signature of the SPP mechanism. On the other hand, a deviation of the temperature dependence of the low-field mobility from the  $1/T$  law is a more subtle evidence for the SPP mechanism, since the position of the threshold voltage can be temperature dependent due to the hysteresis [14, 15]. In addition, the maximum mobility associated with the onset of the scattering in the second subband shows a superlinear temperature dependence ( $\propto T^{1.5}$ ) even for only CNT phonon scattering see Fig. 1 in Supporting Information. At the same time in metallic tubes, the density of states around the neutrality point is constant and, therefore,

a much weaker density dependence of the mobility (or conductance) is expected, which makes the temperature dependence of the mobility to be a more suitable test for the SPP mechanism. Indeed, in metallic tubes, a non-linear temperature dependence of the resistivity has been reported [4].

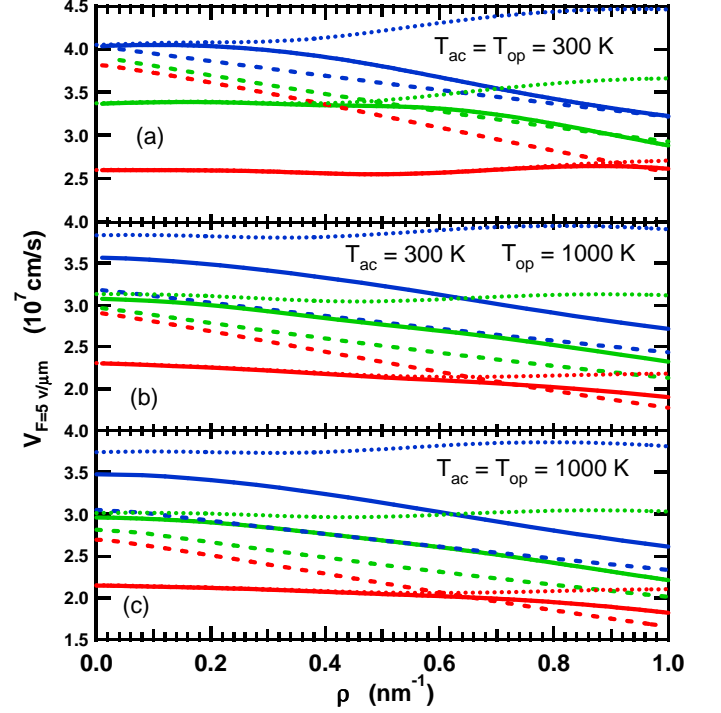


FIG. 6: High field velocity (at  $F = 5$  V/ $\mu$ m) as a function of carrier density in three tubes (13,0)  $d = 1.0$  nm – red, (19,0)  $d = 1.5$  nm – green, (25,0)  $d = 2.0$  nm – blue. Solid curves are obtained with both CNT and SiO<sub>2</sub> phonon scattering, dashed curves with only CNT phonon scattering, and dotted curves with both CNT and SiO<sub>2</sub> phonon scattering, but carriers restricted to the first subband. Polar phonons are kept at  $T = 300$  K, while CNT acoustic and optical phonons are allowed to heat up to (a)  $T_{\text{ac}} = 300$  K  $T_{\text{op}} = 1000$  K, (b)  $T = 1000$  K and (c)  $T_{\text{ac}} = T_{\text{op}} = 1000$  K respectively.

Finally, we discuss the transport properties of semiconducting CNTs under the high bias conditions. At low-densities with only CNT phonon scattering, the drift velocity  $v_{\text{high}}$  was found to saturate with the field  $F$  at about half the Fermi velocity  $v_{\text{sat}} \sim 5 \cdot 10^7$  cm/s (for the choice of  $t_0 = 3$  eV):  $v_{\text{high}}^1 = (v_0 F)^{-1} + v_{\text{sat}}^1$  [7]. As the density increases, the high field velocity drops and density dependence of the velocity does not show a simple saturated form [13]. Here we report high field velocity calculated at a constant  $F = 5$  V/ $\mu$ m, which can be achieved in the experiments before the long channel CNT burns under high bias condition [16, 17, 18]. The results are shown in Fig. 6. The reference dashed lines are calculations with only CNT phonon scattering. As the SPP scattering process is turned on, the high bias velocity drops at small densities, especially in smaller di-



ameter tubes, while it increases at larger densities and larger diameter tubes as shown in Fig. 6a. This is due to both the hyperbolic dispersion of the CNT band structure [19] and the multiband nature of transport at high biases. The SPP scattering is much stronger than the CNT optical phonon scattering and, therefore, the tail of distribution function or effective electronic temperature [20] ( $T_e = eF_{ph}$ ) is expected to be smaller in the presence of the SPP mechanism, due to the shorter mean free path  $\lambda_{ph}$ . We find that at low densities, the first subband dominates transport by using restricted calculations with electrons occupying only the first subband as shown in Fig. 6 (dotted curves). As the density increases, the band velocity increases and so does the drift velocity. In the multiband calculations, the higher subbands with higher effective masses and lower band velocities influence transport, which lowers the drift velocity in Fig. 6 (solid curves). In the presence of only CNT phonon scattering, even at low densities the high bias transport is influenced by higher subbands, which makes the quantitative interpretation to be more difficult although it shows similar trends.

It has been suggested that under high bias conditions the optical phonons can be out of equilibrium with the acoustic CNT phonons [17, 21]. Recently, the non-equilibrium phonon population in CNTs under high bias conditions was directly observed experimentally [22]. To study the influence of the hot phonon effect on the transport properties, we calculate the drift velocity as a function of density for three different tubes in Fig. 6b. In the case of only CNT scattering, we find a significant drop in the drift velocity with the elevation of the optical phonon temperature. This drop gives rise to the negative differential conductance as observed in the suspended CNTs [17]. On the other hand, the magnitude of the drift velocity change in the presence of the SPP is much smaller, because SPP, which dominates transport, are kept at ambient temperature. The weaker effect of the CNT phonons on transport properties leads to near disappearance of the negative differential conductance even when CNT optical phonon temperature is elevated [22]. Finally, we find that the drift velocity under high bias conditions in the presence of the SPP scattering is not affected by the acoustic CNT phonon temperature as is seen from Fig. 6c, which is essentially identical to Fig. 6b.

In conclusion, we calculated the effect of the surface polar phonon scattering on transport in semiconducting CNTs. We find that at room temperature SPP scattering reduces the mobility by an order of magnitude from the intrinsic value determined by the CNT acoustic phonon scattering. The diameter dependence of the mobility in the presence of SPP can still be well approximated by a power law, but with a reduced temperature dependent value of the power as the relative role of the SPP scattering on transport increases with increasing tube diam-

eter. At temperatures above about 100 K, we predict an additional minimum in the mobility-density dependence associated with the low energy SPP phonon scattering. This can serve as an experimental signature of the SPP mechanism. Under high bias conditions we find, counter-intuitively, that SPP scattering may increase the drift velocity, especially in large diameter tubes, high carrier density, and elevated CNT optical phonon temperatures due to the non-parabolicity of the bandstructure and influence of the higher subbands.

Finally, it is useful to comment on the SPP scattering in CNTs on other possible polar gate insulators, such as  $Al_2O_3$ ,  $AlN$ ,  $ZrO_2$ ,  $HfO_2$ , and  $ZrSiO_4$  in which the lowest energy phonon with an appreciable coupling is estimated to be  $\sim \hbar\omega_{TO} = \hbar\omega_{TO} / (1 + \epsilon_0) = \hbar\omega_{TO} / (1 + \epsilon_\infty) = 87, 108, 37, 24, 60$  meV, respectively using the parameters in ref. [9]. The Frohlich couplings Eq. (3) to the low energy modes in these materials are similar to that in  $SiO_2$ . Therefore, we may expect that from the point of SPP scattering,  $AlN$  would be the best choice for the insulator, while  $HfO_2$  and  $ZrO_2$  would give the strongest scattering at room temperature.

---

[\*] Electronic address: vperbein@us.ibm.com

- [1] Avouris, Ph.; Chen, Z.; Perebeinos, V. *Nature Nano* 2007, 2, 605.
- [2] Durkop, T.; Getty, S. A.; Cobas, E.; Fuhrer, M. S. *Nano Lett.* 2004, 4, 35.
- [3] Zhou, X.; Park, J.-Y.; Huang, S.; Liu, J.; McEuen, P. L. *Phys. Rev. Lett.* 2005, 95, 146805.
- [4] Purewal, M. S.; Hong, B. H.; Ravi, A.; Chandra, B.; Hone, J.; Kim, P. *Phys. Rev. Lett.* 2007, 98, 186808.
- [5] Suzuura, H.; Ando, T. *Phys. Rev. B* 2002, 65, 235412.
- [6] Pennington, G.; Goldman, N. *Phys. Rev. B* 2003, 68, 045426.
- [7] Perebeinos, V.; Terso, J.; Avouris, Ph. *Phys. Rev. Lett.* 2005, 94, 086802.
- [8] Petrov, A. G.; Rotkin, S. V. *JETP Lett.* 2006, 84, 156.
- [9] Fischetti, M. V.; Neumayer, D. A.; Cartier, E. A. *J. Appl. Phys.* 2001, 90, 4587.
- [10] Wang, S. Q.; Mahan, G. D. *Phys. Rev. B* 1972, 6, 4517.
- [11] We adopt a back-gate geometry, with one-dimensional CNT lying on two-dimensional polar substrate. Such that we approximate a 2D top dielectric, i.e. CNT in air, by  $\epsilon = 1$ .
- [12] Sano, N. *J. Phys. D* 1989, 22, 309; Lynch, W. J. *J. Appl. Phys.* 1972, 43, 3274; Spitzer, W. G.; Kleinman, D. A. *J. Phys. Rev.* 1961, 121, 1324.
- [13] Perebeinos, V.; Terso, J.; Avouris, Ph. *Nano Lett.* 2006, 6, 205.
- [14] Radosavljevic, M.; Freitag, M.; Thadani, K. V.; Johnson, A. T. *Nano Lett.* 2002, 2, 761.
- [15] Kim, W.; Javey, A.; Vermesh, O.; Wang, Q.; Li, Y.; Dai, H. *Nano Lett.* 2003, 3, 193.
- [16] Chen, J.; Perebeinos, V.; Freitag, M.; Tang, J.; Fu, Q.; Liu, J.; Avouris, Ph. *Science* 2005, 310, 1171.
- [17] Pop, E.; Mann, D. A.; Cao, J.; Wang, Q.; Goodson, K.

- E.; Dai H. Phys. Rev. Lett. 2005, 95, 155505.
- [18] Pop, E.; Mann, D. A.; Goodson, K. E.; Dai, H. J. of Appl. Phys. 2007, 101, 093710.
- [19] McIntire, J. W.; Dunlap, B. I.; White, C. T. Phys. Rev. Lett. 1992, 68, 631.
- [20] Perebeinos, V.; Avouris, Ph. Phys. Rev. B. 2006, 74, 121410(R).
- [21] Lazzeri, M.; Piscanec, S.; Mauri, F.; Ferrari, A. C.; Robertson, J. Phys. Rev. Lett. 2005, 95, 236802.
- [22] Steiner, M.; Freitag, M.; Perebeinos, V.; Tsang, J. C.; Small, J. P.; Kinoshita, M.; Yuan, D.; Liu, J.; Avouris, Ph. Electrical power dissipation in a carbon nanotube transistor. (submitted)